J Mater Sci (2008) 43:5230–5242
DOI 10.1007/s10853-008-2766-z

Evaluation of water degradation of vinylester and epoxy matrix composites by single fiber and composite tests

F. A. Ramirez · L. A. Carlsson · B. A. Acha

Received: 23 April 2008 / Accepted: 30 May 2008 / Published online: 17 June 2008

Abstract Degradation of the mechanical properties of vinylester and epoxy matrix composites exposed to water has been approached by monitoring the strengths of glass and carbon fibers and resins. In addition, the fiber/matrix (F/M) interface strengths and debond lengths of single-fiber composites were determined and test results were compared to test results of macroscopic composite specimens. The single-fiber tensile test results indicate a substantial loss of the tensile strength of glass fibers and the fragmentation tests reveal loss of F/M shear strength and substantial debonding for both glass and carbon fiber composites after water exposure. The transverse strengths of the composites are also degraded to large extents. The tests results identify water degradation of the F/M interface as a major strength limiting mechanism.

Introduction

Fiber-reinforced polymer matrix composites are used in marine applications as they offer several advantages over monolithic materials such as metals, ceramics, and plastics such as low density, high specific stiffness and strength, and lack of corrosion. Glass fiber-reinforced polymer composites are well established although carbon fiber-reinforced composites start to enter this field of application [1]. Currently, due to considerations of cost and ease of processability, low viscosity vinylester resins that may be cured at room temperature (RT) are being used in preference to epoxy resins [2].

There is currently a lack of information concerning the durability of vinylester matrix composite materials, especially those containing carbon fibers. Moisture absorption is a common scenario in polymer matrix composite materials which may lead to a number of undesirable effects, such as degradation of the matrix, fiber, and fiber/matrix (F/M) interface. The chemical nature of the polymer matrix makes it attractive to water. The absorption of water molecules inside the macromolecular network of a thermoset causes swelling (expansional strains) and plasticization of the matrix [3–5]. Plasticization occurs when water molecules break secondary bonds between polar groups, thus partially destroying the mechanical cohesion of the network and increasing the molecular mobility [6]. Plasticization is reflected in reductions of Young's modulus and glass transition temperature (T_g). In addition, polymers subject to water or humid environments are often vulnerable to hydrolysis of unsaturated groups by water [7] and removal of chemical species from the matrix by leaching.

Moisture may also affect the fibers in a composite. For instance, water-immersed glass fibers do not absorb water, although they are susceptible to leaching of soluble oxides [8–13] followed by strength reduction. The rate of degradation of glass fibers is strongly influenced by temperature [9, 13]. Carbon fibers, however, are inert to water and humidity.

The structural integrity of fibrous polymeric composites is also critically dependent on the stability of the F/M interface [14]. A strong adhesion between fiber and matrix assures efficient load transfer; it delays the onset of microstructural damage formation and reduces the rate of

F. A. Ramirez · L. A. Carlsson
Department of Mechanical Engineering, Florida Atlantic University, 777 Glades Road, Boca Raton, FL 33431, USA

B. A. Acha (✉)
Department of Ocean Engineering, Florida Atlantic University, 101 N. Beach Road, Dania Beach, FL 33004, USA
e-mail: bacha@oe.fau.edu

damage accumulation. In addition, a strong F/M adhesion is necessary for material long-term property retention [15]. Absorption of moisture may degrade the F/M interface as a result of either a reduction of the chemical bonding between the fiber and the matrix or a reduction in the residual thermal shrinkage stresses at the F/M interface due to moisture absorbed-induced swelling [16]. Researchers have studied environmental effects on the F/M interface of various composite systems by direct [17–20] and indirect (macromechanical) tests [21–26]. For currently used glass/vinylester and carbon/vinylester composites, the information regarding the effect of seawater on the F/M interface is very limited [3, 16, 25] and further research is justified.

The aim of this work is to experimentally investigate the degradation of the critical components of polymer matrix composites for naval applications subject to distilled and sea water (viz., fiber, matrix, and the F/M interface). The tensile strength of the fibers is monitored using the single filament test (SFT). The matrix materials are characterized by tensile, flexure, and dynamic mechanical tests. The single fiber fragmentation test (SFFT) is used to determine the F/M interface shear strength and extent of F/M debonding. In addition, macroscopic composites are examined using transverse tensile and transverse flexure tests to study the influence of the integrity of the matrix and F/M interface on the macroscopic response.

Materials and specimens

The fibers used in this paper are T700 carbon fibers from Toray with "F" sizing which is specially designed by the manufacturer to be compatible with vinylester resins, AS4 unsized carbon fibers from Hexcel, and E-glass fibers from 3TEX with silane sizing. The fibers are combined with (i) a low cost two part epoxy (MAS) generally used for boat repair, and with the following vinylester resins used is in naval applications, (ii) Ashland Derakane 411-350 vinylester (VE D411) formulated with 1.0 parts per hundred resin weight (phr) of methylethylketone peroxide (MEKP), 0.03 phr of cobalt naphthenate-10% (CoNap 10%), and 0.015 phr of 2,4-Pentanedione (2,4-P), (iii) Ashland Derakane 8084 elastomer modified vinylester (VE D8084) formulated with 1.5 phr of MEKP, 0.18 phr of CoNap 10%, and 0.05 phr of dimethylaniline (DMA), and (iv) Hetron 922L pre-promoted vinylester (VE H922L) formulated with 1.25 phr of MEKP. The properties of these materials as provided by the manufacturers are listed in Table 1.

SFFT specimens

The SFFT employs a single fiber embedded in a resin matrix which is molded into a dog-bone specimen as shown in Fig. 1 [27]. The following fiber and matrix combinations were studied using the SFFT: T700/VE D411, T700/VE D8084, T700/MAS epoxy, AS4/VE H922L, E-glass/VE D8084, and E-glass/MAS epoxy.

A single fiber was carefully selected by hand from a fiber bundle without touching the fibers (except at the ends). Then, the fiber was placed in a silicone rubber SFFT specimen mold with a small amount of rubber cement applied

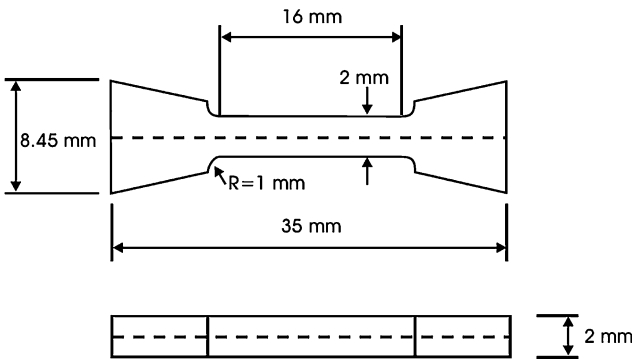

Fig. 1 SFFT specimen [28]

Table 1 Manufacturers' specifications for fiber and matrix materials

	Fiber			Matrix			
	T700	AS4	E-glass	MAS epoxy	VE D411	VE D8084	VE H922L
Modulus (GPa)	230	228	73	2.2	3.2	2.9	3.7
				2.1 ± 0.1[a]	3.1 ± 0.1[a]	2.7 ± 0.1[a]	3.1 ± 0.1[a]
Tensile strength (MPa)	4,900	4,278	3,450	46	86	76	83
				47 ± 3.0[a]	76.8 ± 0.6[a]	58.3 ± 0.6[a]	76.2 ± 1.2[a]
Strain (%) (at failure)	2.1	1.87	4.5	8–9	5–6	8–10	7.9
				8.8 ± 0.8[a]	5.4 ± 1.0[a]	7.8 ± 1.8[a]	5.4 ± 1.3[a]
T_g (°C)	–	–	–	70	120	115	–
Density (g/cm^3)	1.8	1.79	2.54	1.13	1.14	1.14	–

[a] Data measured in this study

at the ends of the sprue to keep the fiber in place. After the fiber was straightened, a small amount of epoxy was added at the sprue to secure the positioning of the fiber and prevent fiber waviness. Then, resin was poured in the mold and allowed to cure at RT. After cure, the SFFT specimens were put in an oven for post-cure. Vinylesters D411 and H922L were post-cured at 120 °C for 2 h, whereas vinylester D8084 was post-cured at 99 °C for 2 h as suggested by the suppliers. The epoxy needed a more complex cyclic post-cure to reach acceptable properties. The post-cure process consisted of cycles where the temperature was kept at 40 °C for 6 h followed by 2 h at RT repeated six times, and six subsequent cycles where the temperature was kept at 60 °C for 6 h followed by 2 h at RT [28].

Composite specimens

Unidirectional composites were made from T700/VE D411, T700/VE D8084, and T700/epoxy. Laminates consisting of four plies were fabricated using vacuum-assisted resin transfer molding at RT and cured for 24 h RT. Then, post-cure was performed depending on the resin as explained in section "Single fiber fragmentation test specimens." The panel thickness after post-cure was 1.2 mm. Transverse test specimens were cut from the unidirectional composite plates. The transverse tensile specimens were 130 mm long and 20 mm wide and the transverse flexure specimens were 50.8 mm long and 12.7 mm wide (ASTM standards D3039 [29] and D790 [30]).

Resin and fiber test specimens

Resin specimens were made from VE D411, VE D8084, VE H922L, and MAS epoxy. 1.2 mm thick resin panels were cast at RT between two glass plates (treated with release agent) and cured for 24 h RT followed by the post-cure specified in section "Single fiber fragmentation test specimens." Then the panels were cut into straight-edge coupons with dimensions 50.8 mm long by 12.7 mm wide for flexure testing, and 30 mm long by 6 mm wide for DMA testing. Dog-bone specimens with a gage length of 50 mm and gage section dimensions of 12 × 3.5 mm^2 were fabricated for tensile testing by pouring the resin into a silicone rubber mold. For the SFT, a single fiber was separated from a tow of fibers and mounted on a cardboard tab as shown in Fig. 2. A gage length of 20 mm was used for this test.

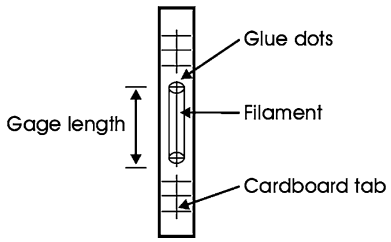

Fig. 2 SFT specimen

Test procedures

Environmental exposure

After post-cure of the specimens, they were considered dry (defining dry conditions). Selected specimens were immersed in water (distilled water at RT and seawater at RT 40 and 60 °C, respectively). The weight change was periodically monitored. Each time a specimen was removed from an immersion tank, it was carefully dried with a paper towel. Then, weight measurement was done using a precision balance. The moisture content, M (in percent), is calculated using

$$M\% = \frac{W_t - W_o}{W_o} \times 100, \quad (1)$$

where W_t is the measured weight of the specimen at time t and W_o is the specimen initial dry weight.

Material characterization

Tensile tests on the resins were conducted at dry conditions only using dog-bone specimens according to ASTM D638 [31]. The tensile failure strain is extremely important since the SFFT requires a ductile matrix in order to reach saturation of fiber breaks before matrix cracking. The test was performed in an MTS Insight 50 universal testing machine at a crosshead speed of 2 mm/min. An extensometer with 25.4-mm gage length was used to measure the strain.

Flexure tests on dry and wet neat resin specimens were conducted according to ASTM D790 [30]. The tests were conducted in a small three-point bending stage equipped with a 200 N load cell at a crosshead rate of 1 mm/min, and support span of 23 mm. The flexural strength, σ_F, is calculated from classical beam theory

$$\sigma_F = \frac{3PL}{2wh^2}, \quad (2)$$

where P is the failure load, L the span length, h the thickness, and w is the specimen width.

DMA flexure tests were conducted on dry and wet neat resin specimens according to ASTM D4065 [32] to determine the storage modulus, E' and glass transition temperature, T_g. A Q800 dynamic mechanical analyzer (TA) was used. The measurements were carried out in three-point-bending over a temperature range from −5 °C to well above T_g at a heating rate of 5 °C/min and a fixed frequency of 1 Hz.

The SFT, ASTM D3379 [33], was used to determine the tensile strength of dry and water immersed fibers. Tensile testing was performed at a crosshead speed of 0.5 mm/min in an MTS Insight 1 universal testing machine equipped with a 2 N capacity load cell.

The fiber volume fraction of composites was determined by hot nitric acid digestion of the matrix according to ASTM Standard D3171 [34] and by photomicrographic technique [35]. For the acid digestion method, the weights of the fibers and matrix, W_f and W_m, were determined. The fiber volume fraction, v_f, assuming no voids, is given by:

$$v_f = \frac{\rho_m W_f}{\rho_f W_m + \rho_m W_f}, \tag{3}$$

where ρ_f and ρ_m are the fiber and matrix densities, respectively.

For the photomicrographic method, a surface cut perpendicular to the fiber direction was carefully polished. Then, the polished specimens were examined in the ESEM and optical microscopes, and photographs with high magnification were taken from different regions of the specimen. The areal fractions of fibers and matrix were determined using computer software. v_f is given by:

$$v_f = \frac{A_f}{A}, \tag{4}$$

where A_f and A are the total fiber area and the area of the selected region of the micrograph, respectively.

SFFT and composite tests

The SFFT was conducted on dry and wet specimens. The SFFT specimen, Fig. 1, was loaded in tension using a small hand-operated tensile stage. In the SFFT, the fiber axial stress is introduced through interfacial shear stresses acting parallel to the fiber [36]. The axial fiber stress increases from 0 at the ends and assumes constant stress over most of its length. At a certain level of applied load, the fiber will fracture. If the loading is continued, shear stresses at the F/M interface near the fiber break will transfer load into the broken fiber and repetition of the failure process will occur until the remaining fiber fragments are so short that the shear stress transfer becomes insufficient to cause any further break. This state is called break saturation, and the final fragmentation length is referred to as the *critical length*, l_c. A stronger bond between fiber and matrix increases the transfer rate of load and results in a shorter critical fragment length.

Based on the measured lengths of the fiber fragments, it is possible to estimate the shear strength, τ, of the F/M interface. It is realized that a fiber may be considered as consisting of several links, each containing a flaw of varying severity. A long fiber has a higher probability of encountering a more severe flaw along the fiber length and should be weaker than a short fiber. The fragment length is a statistical quantity described by a two-parameter Weibull distribution analysis which leads to the following expression for the F/M interface shear strength [37]:

$$\tau = \frac{\sigma_f}{2\beta}\Gamma\left(1 - \frac{1}{\alpha}\right), \tag{5}$$

where α and β are the Weibull shape and scale parameters, respectively, and Γ is the Gamma function. In order to determine the fiber strength at the critical fragment length, which is usually <1 mm, using the SFT [33] is virtually impossible; therefore, fibers with larger gage lengths, l_o, are tested and the results are subsequently extrapolated to the critical length, l_c, using the Weibull weakest link theory [38],

$$\sigma_f = \bar{\sigma}_o \left(\frac{l_c}{l_o}\right)^{-1/w}, \tag{6}$$

where $\bar{\sigma}_o$ and σ_f are the fiber tensile strength at gage lengths, l_o and l_c, respectively, and w is the Weibull shape parameter.

Besides fiber fractures, debonding between fiber and matrix typically occurs near the fiber break. Fiber breaks and F/M debonding were examined during SFFT testing using photoelastic patterns observed in optical transmission microscopy (Olympus BX41 with a QICAM-FAST 1394 camera). The region around a fiber break exhibits a colored pattern called birefringence. This phenomenon is caused by shear stresses in the matrix [39]. Theoretically, the highest shear stress at the F/M interface should occur at or near the end of the fragment. In reality, however, this high shear stress causes debonding between fiber and matrix near the fiber break in effect reducing the shear stress transfer at the

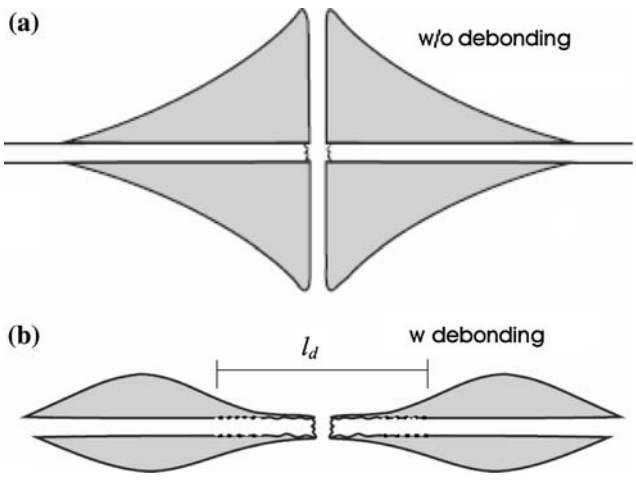

Fig. 3 Schematic feature of photoelastic birefringence of shear stress around a fiber break without debonding (**a**) and with debonding (**b**). After Kim and Nairn [40]

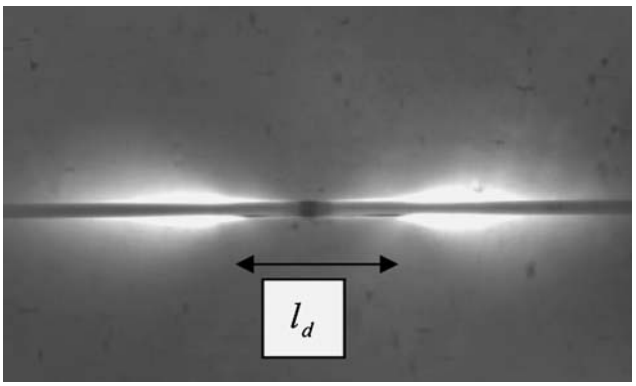

Fig. 4 Picture of fiber fragment and debond length

interface. Figure 3 shows a schematic of the birefringence patterns near a fiber break for the cases of no F/M debonding and some extent of F/M debonding. Figure 4 shows actual photoelastic patterns associated with a fiber break and debonding. Birefringence patterns were therefore used to identify both fiber breaks and debond regions at each fiber break. A computer software (Q-capture Pro) was used to measure fiber fragment and debond lengths.

Dry and wet composite specimens were tested in transverse tension and flexure. The transverse tensile test, ASTM D3039 [29], was conducted in an MTS Insight 1 testing machine with a 1 kN load cell at a crosshead rate of 0.5 mm/min. The transverse flexure test was conducted in a three-point fixture at a support span of 23 mm in a small loading stage (Gatan, microtest 200) with a 200 N load cell at a crosshead rate of 1 mm/min. The flexural strength is calculated from Eq. 2.

Results and discussion

Water absorption

Figure 5 illustrates the curves of weight change of the neat resin specimens in seawater (at RT and elevated temperatures) versus square root of immersion time.

The epoxy specimens absorb much more moisture than the vinylester specimens. For the vinylester resins, the pre-promoted (VE H922l) and rubber-modified (VE D8084) vinylesters absorbed about twice as much moisture as VE D411. It can be also noticed that exposure to water at higher temperatures leads to higher slopes of the initially linear portion of the curve indicating a higher rate of moisture transport. This phenomenon occurs since water diffusion is a thermally activated process [41].

Figures 6–8 depict moisture absorption curves for the SFFT and composite specimens immersed in seawater (at RT and elevated temperatures). The maximum moisture contents for neat resins and composites are listed in

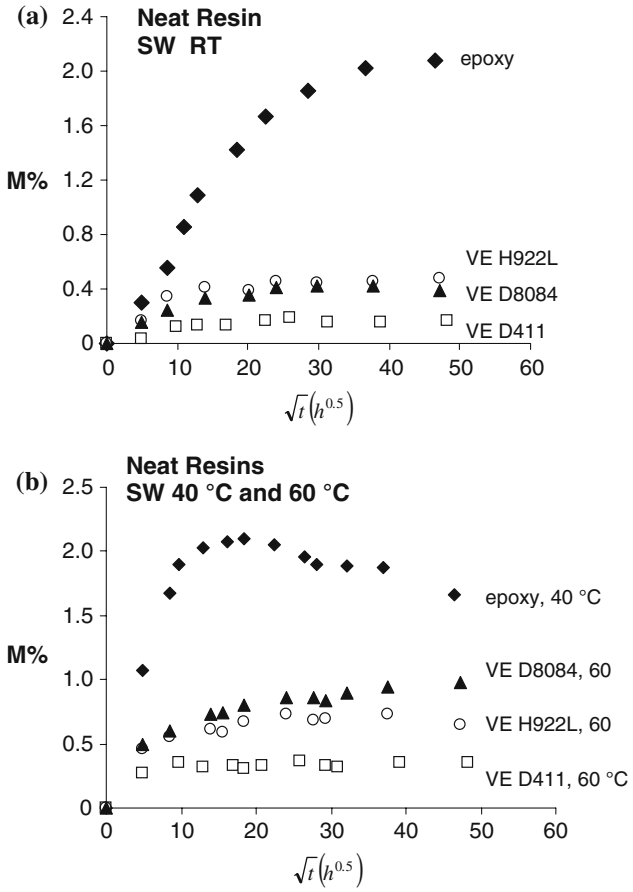

Fig. 5 Weight change for neat resin specimens in seawater as function of square root of immersion time. (**a**) RT and (**b**) 40 and 60 °C

Table 2. The T700/VE D411 composite specimens absorbed more moisture than the neat VE D411 resin specimens; T700/VE D8084 composite specimens absorbed about the same amount of moisture as the neat VE D8084 resin specimens, while T700/epoxy composite specimens absorbed less moisture than the neat epoxy resin specimens. Taking into account the fact that the composites contain only about 36% resin (see section "Composite tests") and that carbon fibers do not absorb water, moisture absorption along the F/M interface (wicking) and possibly through cracks and voids in the material becomes evident. The photomicrographs (data not shown), however, indicate no significant cracks or voids, and wicking is the only remaining mechanism. At maximum moisture content state, the water absorbed by the resin in the transverse flexure composite specimen should be 36% of the water absorbed by the neat resin specimen. The balance moisture content is assumed to be absorbed by wicking. Based on the moisture content results in Table 2 and the wicking analysis presented in the Appendix, the percentages of moisture absorbed by the resin and by wicking were calculated. The results in Table 2 show that the epoxy resin

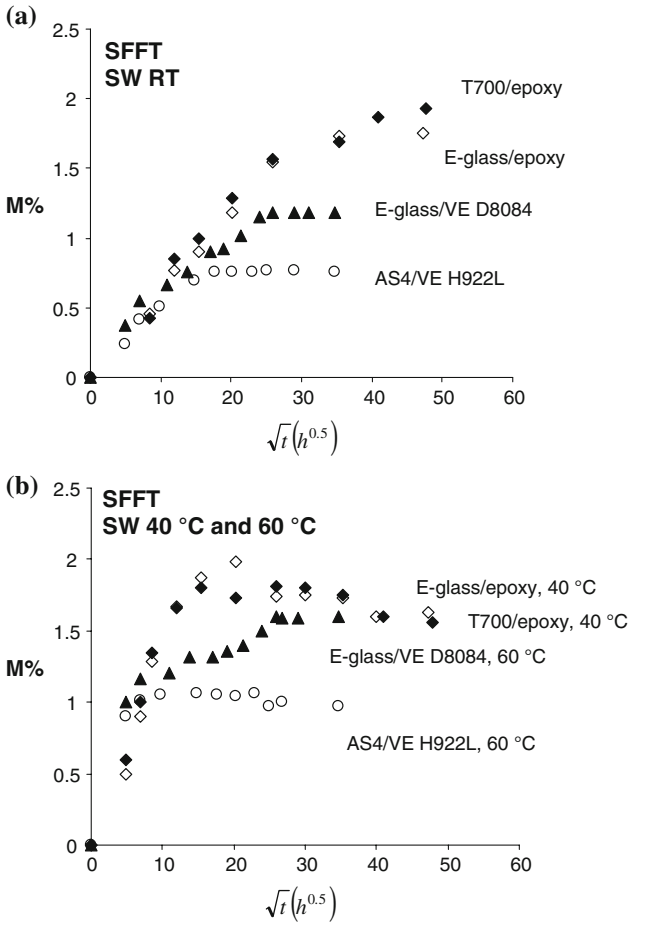

Fig. 6 Weight change for SFFT specimens in seawater as function of square root of immersion time. (**a**) RT and (**b**) 40 and 60 °C

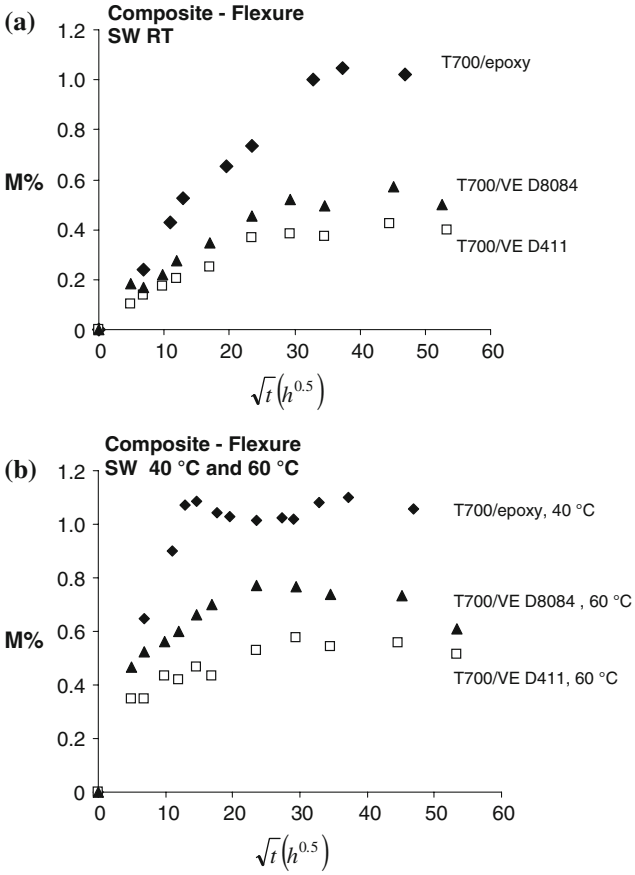

Fig. 7 Weight change for transverse flexure composite specimens in seawater as function of square root of immersion time. (**a**) RT and (**b**) 40 and 60 °C

absorbed about 50% of the total while for the vinylester matrix composites the F/M interface absorbed the major part of the moisture. For the T700/VE D411 composite specimen, wicking accounted for 90% of the water absorbed. These results suggest that the carbon fiber-reinforced vinylester composites have a relatively open and possibly weak interface.

Material mechanical behavior

Figure 9 presents representative tensile stress–strain curves of the various resins at dry conditions. Vinylester D411 and pre-promoted VE H922L resins present extremely similar stress–strain curves and high strength (around 76 MPa), but their low strain to failure (5.4%) makes the SFFT challenging. On the other hand, the elastomer-modified vinylester (VE D8084) and the epoxy resins present lower strengths but higher ductility which potentially should make them suitable for the SFFT. Mechanical properties determined from the tests, listed in Table 1 (with an 'a'), agree closely with those provided by the manufacturers.

Table 3 presents DMA and flexure test results of neat resin specimens tested at dry conditions and after 1300 h of immersion in water. The T_g results (at dry conditions) obtained in this study are consistent with those values reported by the manufacturers (see Table 1). The results in Table 3 show that the vinylester matrices are not significantly affected by exposure to water. The epoxy, however, underwent extensive degradation (i.e., modulus, strength, and T_g) after exposure to water at 40 °C. This may possibly be related to the high water absorption by the epoxy resin (Fig. 5).

Table 4 summarizes the strength data for carbon and E-glass fibers at dry conditions; where σ_o and w are the Weibull scale and shape parameters, respectively. A graph of E-glass fiber strength versus time of exposure to water is shown in Fig. 10. The E-glass fibers are dramatically weakened by exposure to seawater, especially at elevated temperatures. For instance, E-glass fibers exposed to seawater at 60 °C lost 50% of their strength after 2 days of exposure. Carbon fibers, on the other hand, were found to be inert to water exposure. The E-glass fiber strength degradation was predicted fitting the experimental data to the following expression [13]:

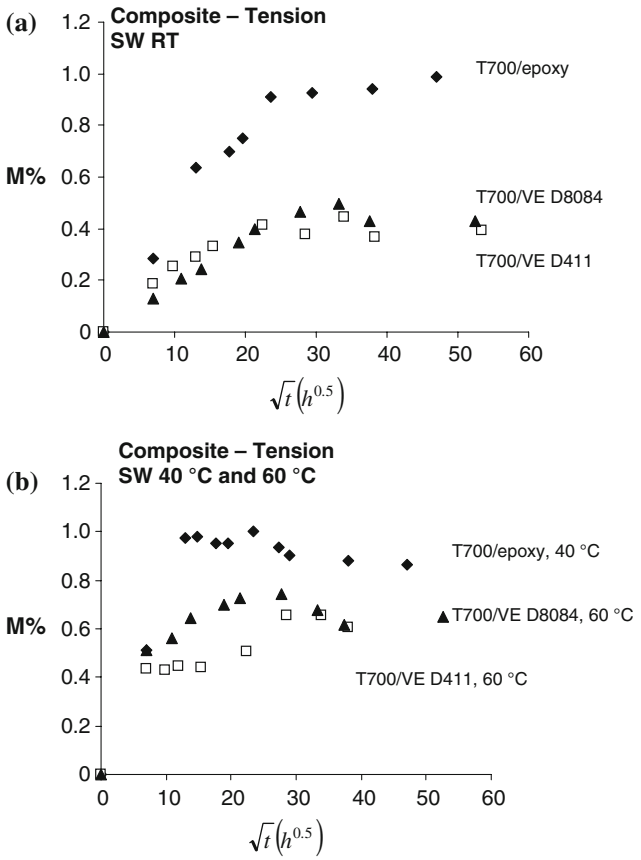

Fig. 8 Weight change for transverse tensile composite specimens in seawater as function of square root of immersion time. (**a**) RT and (**b**) 40 and 60 °C

Table 2 Maximum moisture contents

Systems	Conditioning	Neat resin	Composite		
		M (%)	*M* (%)	Resin (%)	F/M interface (%)
Epoxy and T700/epoxy	DW RT	2.10	0.83	58	42
	SW RT	2.02	0.92	51	49
	SW 40C	2.09	1.00	48	52
VE D411 and T700/VE D411	DW RT	0.25	0.55	10	90
	SW RT	0.19	0.44	10	90
	SW 40C	0.33	0.59	13	87
	SW 60C	0.37	0.65	13	87
VE D8084 and T700/VE D8084	DW RT	0.49	0.59	19	81
	SW RT	0.42	0.50	19	81
	SW 40C	0.58	0.64	21	79
	SW 60C	0.94	0.74	29	71

$$\sigma(t) = \bar{\sigma}_o(1 + At)^{-B}, \tag{7}$$

where A and B are the fitting parameters as given in Table 5 and t is time of immersion in seconds.

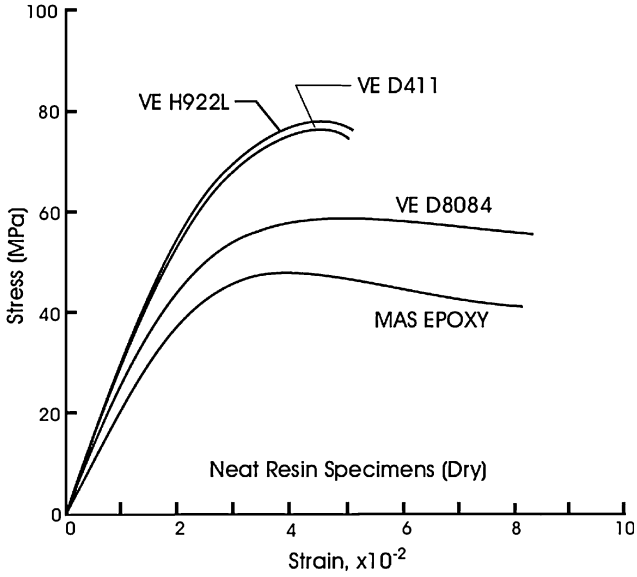

Fig. 9 Tensile stress–strain curves for neat resin specimens

Single fiber fragmentation test

Figure 11 presents typical birefringence patterns near a fiber break at the fiber break saturation state for E-glass/VE D8084 and E-glass/epoxy SFFT specimens at dry (top) conditions and after 1300 and 2100 h of immersion in water, respectively (bottom). Both systems presented significant decline of the photoelastic pattern intensity and large extents of F/M debonding after exposure to water. Results for interface shear strength and debond lengths for E-glass/VE D8084 and E-glass/MAS epoxy are presented in Tables 6 and 7. Notice that the calculation of the F/M interface shear strength (Eq. 5) accounts for the glass fiber strength degradation after immersion in water (Eq. 7). For this analysis, it is assumed that the E-glass fiber in the SFFT specimen is equally degraded by water as if the fiber was isolated. The results show that the F/M interface shear strength of both systems is substantially reduced after immersion in water. The interface shear strengths of E-glass/VE D8084 and E-glass/epoxy were reduced by about 75%.

Figure 12 shows typical birefringence patters at the fiber break saturation state for carbon T700/epoxy SFFT specimens at dry conditions and after 2100 h of immersion in water. These birefringence patterns show an extremely large increment of debond length as indicated by the significant decline of photoelastic intensity after exposure to water. SFFT results for T700/epoxy specimens are listed in Table 8. The F/M interface shear strength of this system was reduced by 82% while the debond length was increased by a factor of 20 in the worst case. Since carbon fibers do not degrade when subject to water, the reduction of F/M interface shear strength is not intermixed with degradation of the fiber.

Table 3 Neat resin storage modulus, flexure strength, and glass transition temperature at dry and wet conditions

	MAS epoxy				VE D411			
	M%	E_f' (GPa)	σ_f (MPa)	T_g (°C)	*M*%	E_f' (GPa)	σ_f (MPa)	T_g (°C)
Dry	–	2.8 ± 0.0	68.5 ± 2.1	66.1 ± 0.7	–	2.9 ± 0.1	132 ± 1.3	118 ± 0.4
DW RT	2.10	2.4 ± 0.1	42.5 ± 3.7	64.2 ± 1.3	0.25	2.9 ± 0.1	124 ± 0.9	117 ± 1.4
SW RT	2.02	2.1 ± 0.0	38.9 ± 3.6	55.3 ± 0.3	0.19	3.0 ± 0.2	126 ± 1.4	116 ± 2.0
SW 40C	2.09	2.3 ± 0.1	31.3 ± 2.1	46.8 ± 1.2	0.33	2.9 ± 0.3	132 ± 4.5	117 ± 0.5
SW 60C	–	–	–	–	0.37	3.0 ± 0.0	129 ± 4.6	119 ± 0.4
	VE D8084				VE H922L			
	M%	E_f' (GPa)	σ_f (MPa)	T_g (°C)	*M*%	E_f' (GPa)	σ_f (MPa)	T_g (°C)
Dry	–	2.9 ± 0.1	117 ± 1.1	120 ± 1.1	–	2.9 ± 0.3	135 ± 4.8	118 ± 5.7
DW RT	0.49	2.9 ± 0.0	108 ± 1.5	119 ± 0.2	0.49	3.0 ± 0.1	128 ± 3.4	122 ± 1.8
SW RT	0.42	3.1 ± 0.1	107 ± 0.6	118 ± 0.6	0.45	3.1 ± 0.3	127 ± 2.3	117 ± 4.9
SW 40C	0.58	3.1 ± 0.2	112 ± 1.8	117 ± 0.6	0.60	3.2 ± 0.2	134 ± 1.1	116 ± 6.0
SW 60C	0.94	3.2 ± 0.0	117 ± 1.3	118 ± 0.9	0.73	2.8 ± 0.1	132 ± 4.5	115 ± 6.2

Table 4 Single fiber strength (at 20-mm gage length)

	E-glass	T700	AS4
Diameter (μm)	14 ± 0.5	6.9 ± 0.3	7.1 ± 0.3
Strength (MPa)	2,060 ± 353	4,400 ± 905	4,560 ± 636
σ_o (MPa)	2,200	4,760	4,820
W	6.85	5.62	9.17

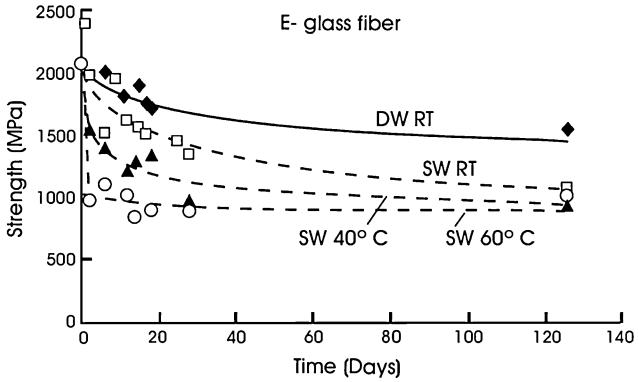

Fig. 10 Tensile strength of E-glass fiber after immersion in water

Table 5 Fitting parameters for predicting E-glass fiber degradation by exposure to water

	A (1/s)	*B*
DW RT	2.30E−06	0.11
SW RT	2.01E−06	0.22
SW 40 °C	3.83E−05	0.13
SW 60 °C	2.11E+02	0.04

Typical birefringence patterns at the fiber break saturation state for AS4/VE H922L SFFT specimens at dry conditions and after 1300 h of exposure are shown in Fig. 13. The low intensity of the birefringence patterns shows that the system has a very weak F/M interface even at dry condition. The birefringence patterns for the specimen tested after immersion in water at RT were extremely weak making it difficult to identify the fiber breaks. For the AS4/VE H922L SFFT specimens tested after immersion in seawater at elevated temperatures, the photoelastic effects were not detectable implying excessive debonding and therefore it was not possible to identify the fiber breaks and quantify debonds lengths. The weak F/M interface may be attributed to the fact that the AS4 carbon fiber was unsized. SFFT results for AS4/VE H922L are listed in Table 9. For the specimens subjected to water at RT, the F/M interface shear strength was reduced by 63%, while the debond length was increased by a factor of 6.

The SFFT results are summarized in Fig. 14. The E-glass systems performed better in water than the carbon systems (using current fiber sizing) in terms of retention of the F/M interface shear strength and debonding. However, it should be kept in mind that E-glass fibers degrade by exposure to water, especially at elevated temperatures (see Fig. 10).

The SFFT was unsuccessful for T700/VE D411 and T700/VE D8084 systems. The T700/VE D411 specimens failed before reaching saturation of fiber breaks due to the brittle nature of this vinylester resin. The few breaks that occurred before specimen failure presented weak birefringence patterns indicating a poor F/M interface. The T700/VE D8084 specimens presented excessive debonding and extremely weak birefringence patterns making it very difficult to

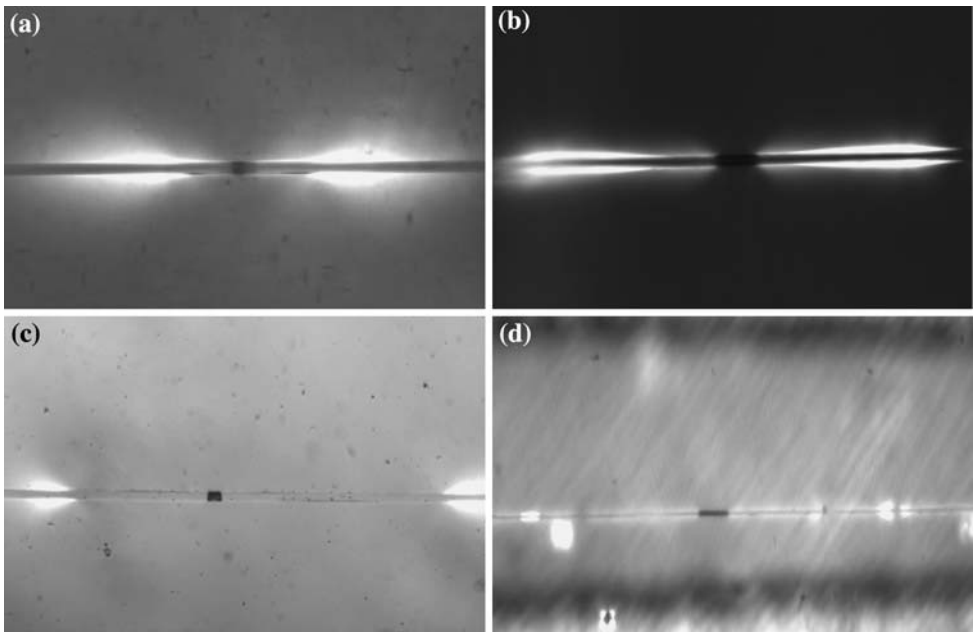

Fig. 11 Birefringence patterns at fiber break saturation for glass fiber SFFT specimens; (**a**) dry E-glass/VE D8084, (**b**) wet E-glass/VE D8084, (**c**) dry E-glass/epoxy, (**d**) wet E-glass/epoxy

Table 6 SFFT results for E-glass/VE D8084

E-glass/VE D8084	*M*%	l_c (μm)	σ (l_c) (MPa)	τ (MPa)	l_d (μm)
Dry	–	440 ± 118	3,600	63.0 ± 25.1	138 ± 97
DW RT	1.13	482 ± 161	2,740	46.4 ± 26.5	222 ± 113
SW RT	1.19	576 ± 184	2,570	35.9 ± 18.9	342 ± 174
SW 40 °C	1.27	728 ± 270	1,660	19.5 ± 13.9	636 ± 310
SW 60 °C	1.70	654 ± 197	1,320	16.0 ± 7.7	546 ± 266

Table 7 SFFT results for E-glass/epoxy

E-glass/epoxy	*M*%	l_c (μm)	σ (l_c) (MPa)	τ (MPa)	l_d (μm)
Dry	–	834 ± 213	3,280	29.9 ± 11.0	132 ± 61
DW RT	1.82	1,660 ± 397	1,610	7.3 ± 2.4	1270 ± 473
SW RT	1.77	1,260 ± 363	1,570	9.8 ± 4.3	862 ± 453
SW 40 °C	1.98	924 ± 376	1,170	11.3 ± 10.1	413 ± 384

Table 8 SFFT results for T700/epoxy

T700/epoxy	*M*%	l_c (μm)	σ (l_c) (MPa)	τ (MPa)	l_d (μm)
Dry	–	860 ± 219	7,970	35.3 ± 12.9	155 ± 77
DW RT	1.92	2,690 ± 603	6,280	8.7 ± 2.7	2,280 ± 1,270
SW RT	1.93	2,790 ± 527	6,240	8.2 ± 2.0	2,190 ± 1,070
SW 40 °C	1.82	3,540 ± 679	5,980	6.2 ± 1.5	3,180 ± 1,330

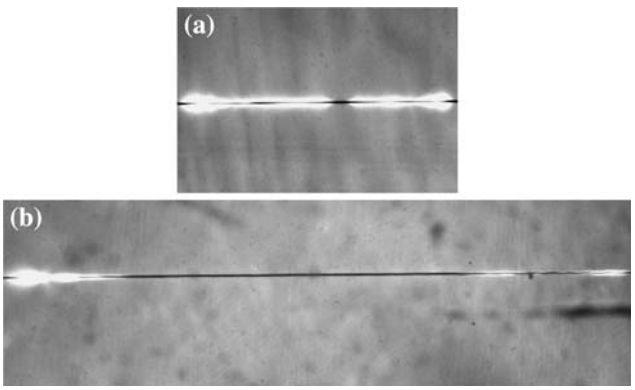

Fig. 12 Birefringence patterns at fiber break saturation for T700/epoxy SFFT specimens (**a**) dry and (**b**) wet

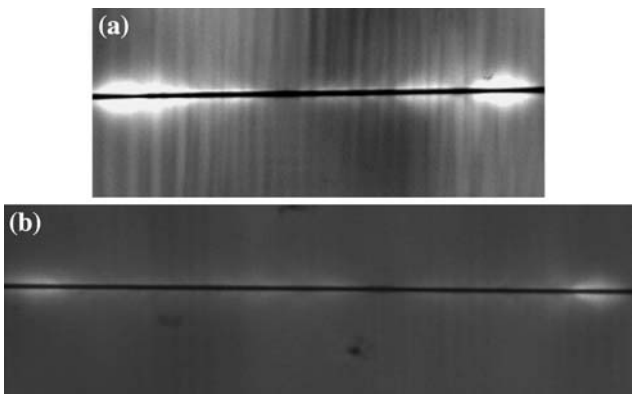

Fig. 13 Birefringence patterns at fiber break saturation for AS4/VE H922L SFFT specimens (**a**) dry and (**b**) wet

Table 9 SFFT results for AS4/VE H922L

AS4/VE H922L	$M\%$	l_c (μm)	σ (l_c) (MPa)	τ (MPa)	l_d (μm)
Dry	–	465 ± 138	6,870	59.1 ± 27.6	145 ± 87
DW RT	0.87	989 ± 262	6,330	24.9 ± 9.7	740 ± 316
SW RT	0.77	1,080 ± 221	6,270	21.8 ± 5.9	835 ± 190

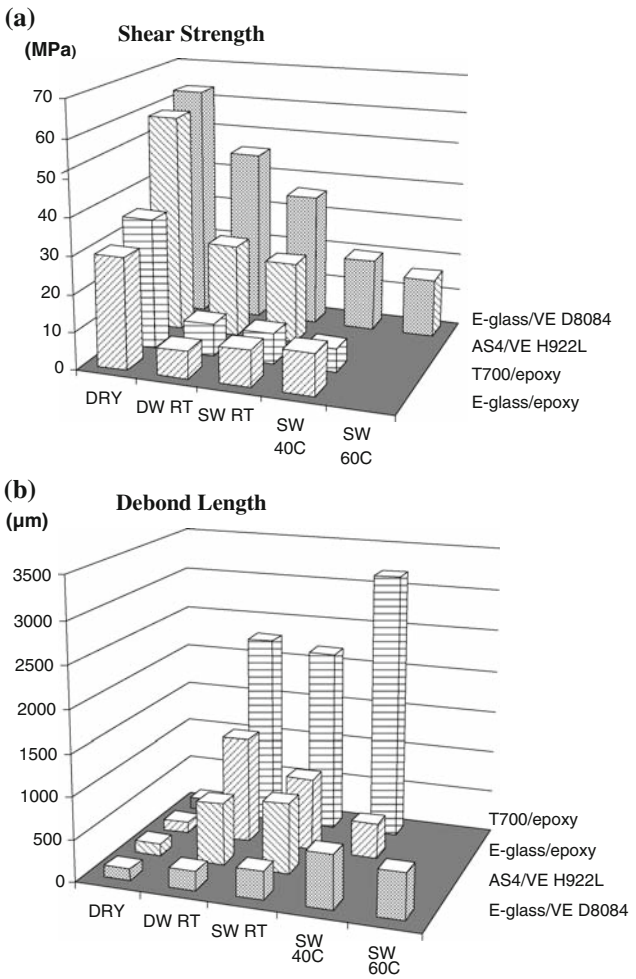

Fig. 14 F/M interface shear strength (**a**) and debond length (**b**) of various systems exposed to water

identify and examine fiber breaks (dry conditions); thus, implying that this system has a poor F/M interface.

Composite tests

The fiber volume fraction of the composites obtained by acid digestion and photomicrographic methods is about 64%. Transverse tensile and flexure tests were performed on dry and wet specimens. T700/VE D411 and T700/VE D8084 specimens were tested in transverse tension after 2000 h of immersion in water while T700/epoxy specimens were tested after 1400 h of exposure. For flexure testing, T700/VE D411 and T700/VE D8084 specimens were tested after 900 h of immersion in water while T700/epoxy specimens were tested after 800 h of exposure. The transverse tensile modulus and strength results are listed in Table 10 and the transverse flexure strength results are listed in Table 11. The transverse test results are summarized in Fig. 15. After water immersion, the epoxy matrix composite experienced large reductions in transverse tensile modulus (about 56%), while the transverse tensile moduli of the vinylester matrix composites were much less affected.

In general, transverse tensile strengths are much lower than transverse flexure strengths. In the transverse flexure test the maximum tensile stress occurs only along a line across the tensile surface at the specimen midspan, while in the transverse tensile test the maximum stress occurs uniformly over the entire cross section and length of the specimen. Therefore, the transverse flexure specimen is much less sensitive to flaws and stronger than the transverse tensile specimens [42]. At dry conditions, the tensile and flexure strengths of the composites are much less than that for the neat resins (see Fig. 9 and Table 3). For T700/epoxy and T700/VE D411 the transverse tensile and flexure strengths are only about 24 and 30% of the tensile and flexure strengths of the resins, respectively. The transverse tensile and flexure strengths of T700/VE 8084 are about 37 and 42% of the resin tensile and flexure strengths, respectively. The higher transverse strength of this system may be due to the high matrix ductility which would prevent flaw propagation in the composite.

Large reductions in transverse tensile and flexure strengths after water immersion were found for all composites. The transverse tensile and flexure strengths of the T700/epoxy composite were reduced by ~60 and 30%, respectively. The transverse tensile and flexure strengths of the T700/VE D411 composite were reduced by 36 and 30%, respectively, while the transverse tensile and flexure strengths of the T700/VE D8084 composite were reduced by 40 and 45%, respectively. The composites with vinylester matrices experienced more strength reduction after immersion in water at elevated temperatures. The transverse strength of the epoxy matrix composite was equally degraded by all environments. Any reduction due to moisture absorption of the transverse strength that is beyond the degradation of the matrix is attributed to F/M interface strength reduction [21]. Inspection of the flexural

Table 10 Transverse tensile modulus and strength of dry and moisture-saturated composites

	T700/MAS			T700/VE D411			T700/VE D8084		
	M%	E_2^T (GPa)	X_2^T (MPa)	*M*%	E_2^T (GPa)	X_2^T (MPa)	*M*%	E_2^T (GPa)	X_2^T (MPa)
Dry	–	5.4 ± 0.5	11.1 ± 2.1	–	7.4 ± 0.4	17.7 ± 1.3	–	7.0 ± 0.4	21.3 ± 3.7
DW RT	1.07	2.4 ± 0.5	5.0 ± 0.5	0.41	8.1 ± 0.6	14.0 ± 3.4	0.60	6.7 ± 0.7	14.5 ± 1.4
SW RT	1.05	2.9 ± 0.6	4.2 ± 0.9	0.42	7.3 ± 0.3	12.5 ± 3.4	0.57	6.4 ± 0.5	15.8 ± 1.7
SW 40 °C	1.10	2.8 ± 0.8	4.3 ± 1.3	0.50	7.6 ± 0.6	14.0 ± 2.6	0.78	6.7 ± 0.4	14.5 ± 1.8
SW 60 °C	–	–	–	0.58	7.3 ± 0.7	11.4 ± 2.0	0.77	6.3 ± 0.5	12.9 ± 1.8

Table 11 Transverse flexure strength of dry and moisture-saturated composites

	T700/MAS		T700/VE D411		T700/VE D8084	
	M%	X_2^F (MPa)	*M*%	X_2^F (MPa)	*M*%	X_2^F (MPa)
Dry	–	21.4 ± 3.5	–	39.1 ± 5.7	–	49.2 ± 5.2
DW RT	0.83	14.8 ± 1.9	0.55	30.6 ± 5.6	0.59	33.2 ± 6.2
SW RT	0.92	16.4 ± 1.9	0.44	31.3 ± 2.3	0.50	38.7 ± 3.1
SW 40 °C	1.00	15.0 ± 1.2	0.59	34.2 ± 4.6	0.64	29.3 ± 4.5
SW 60 °C	–	–	0.65	25.6 ± 6.0	0.74	27.0 ± 4.1

strength data for the resins in Table 3 reveals that only the epoxy resin is degraded by water absorption. Hence, the large transverse strength reduction observed for the vinylester matrix composites must be attributed to loss of F/M interface strength, in agreement with the SFFT results in Tables 6–9.

Conclusions

The objective of this work was to experimentally investigate mechanisms responsible for water degradation of marine type composites. In general, neat epoxy absorbed much more water than neat vinylester. The vinylester matrix composites absorbed more moisture than the neat resins, which was not expected because the resin volume fraction is only about 36% and the carbon fibers do not absorb water. The epoxy matrix composites, on the other hand, absorbed less moisture than the neat epoxy resin, but more than expected based on the 36% resin volume fraction. The difference in moisture absorption behavior between composites and neat resins are attributed for wicking as a water absorbing mechanism.

The flexure test performed on the neat resins show that the vinylester matrices were not significantly affected by exposure to water while the strength of the epoxy was reduced by a factor of 2. Single fiber fragmentation testing revealed large extents of F/M debonding and substantial reductions in the F/M interface shear strength of all systems after exposure to water. The E-glass systems

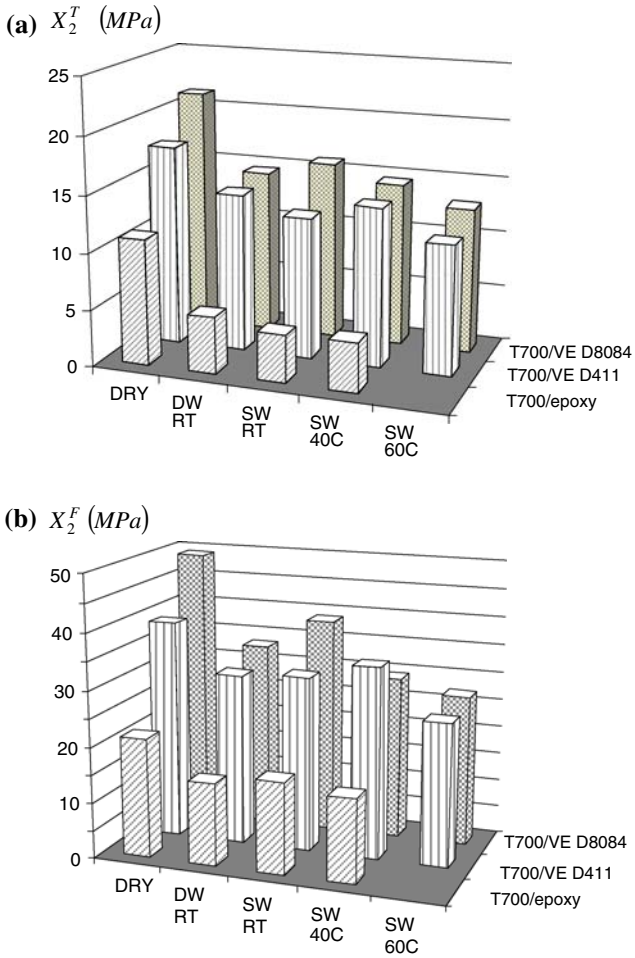

Fig. 15 Transverse strengths of composites exposed to water. (**a**) Tensile strength, (**b**) flexure strength

performed better than the carbon systems in terms of retention of the F/M interface shear strength and debonding, but it was found that E-glass fibers degrade by exposure to water, especially at elevated temperatures.

Transverse tensile and flexure tests were performed on composite specimens to monitor the influence of F/M interface on macroscopic behavior. At dry conditions, each composite displayed a transverse strength much below the strength of the neat resin implying a weak F/M interface

already at dry conditions. In addition, large reductions in transverse strength of the water immersed composites were experienced for all systems as a result of matrix and F/M interface degradation by water. The single-fiber and composite tests results are both supportive of water degradation of the F/M interface as a major mechanism for loss of performance of the composites.

Acknowledgements The support of Office of Naval Research (ONR) under contract No. N00014-05-1-0341managed by Dr. Yapa Rajapakse is gratefully acknowledged. Thanks are due to M. Rich and L.T. Drzal of MSU for SFFT advise.

Appendix: analysis of wicking

Consider a polymer matrix composite. At dry conditions, the weight of the composite, $W_{c,dry}$, is given by:

$$W_{c,dry} = W_m + W_f, \tag{A1}$$

where W_f and W_m are the weights of the fibers and matrix, respectively, in the composite,

$$W_f = \rho_f V_c v_f, \tag{A2a}$$

$$W_m = \rho_m V_c v_m, \tag{A2b}$$

where ρ_f and ρ_m, v_f, and v_m are the fiber and matrix densities and volume fractions, respectively, and V_c is the volume of the composite.

At the maximum moisture content, the weight of the composite $W_{c,max}$, is given by:

$$W_{c,max} = W_m + W_f + W_{w,abs}, \tag{A3}$$

where $W_{w,abs}$ is the weight of water absorbed by the composite,

$$W_{w,abs} = W_{c,dry} M_c, \tag{A4}$$

and M_c is the composite maximum moisture content. Notice that the composite can absorb water through the matrix and interface,

$$W_{w,abs} = W_{wm} + W_{wi}, \tag{A5}$$

where W_{wm} and W_{wi} are the weights of the water absorbed by the matrix and interface, respectively. The weight of the water absorbed by the matrix is given by:

$$W_{wm} = \rho_w V_c v_m M_m \tag{A6}$$

where ρ_w is the density of water and M_m is the maximum moisture content for a neat resin specimen.

Therefore, the weight of water absorbed by the interface (wicking) is given by:

$$W_{wi} = W_{c,dry} M_c - \rho_w V_c v_m M_m. \tag{A7}$$

Finally, the weight fractions of the water absorbed through the matrix, w_{wm}, and by wicking, w_{wi}, are given by:

$$W_{wm} = \frac{\rho_w v_m}{(\rho_f v_f + \rho_m v_m)} \frac{M_m}{M_c}, \tag{A8a}$$

$$W_{wi} = 1 - \frac{\rho_w v_m}{(\rho_f v_f + \rho_m v_m)} \frac{M_m}{M_c}. \tag{A8b}$$

References

1. Kootsookos A, Mouritz AP (2004) Compos Sci Technol 64:1503. doi:10.1016/j.compscitech.2003.10.019
2. Karabhari VM, Zhang S (2003) Appl Compos Mater 10:19. doi:10.1023/A:1021153315780
3. Bradley WL (1995) J Mater Sci 30:5537. doi:10.1007/BF00351570
4. Pomies F, Carlsson LA, Gillespie JW Jr (1995) ASTM STP 1230, Philadelphia
5. Springer GS (ed) (1981) Environmental effects on composite materials. Technomic, CA
6. Verdu J (1984) Water action (In French), in Les Techniques de l'Ingenieur, Volume Plastiques Ref. A 3165, ANFOR, Paris
7. Augl JM, Berger AE (1976) Proceedings of 8th national SAMPE technical conference, California, p 283
8. Otto WH (1966) The effects of moisture on the strength of glass fibers—a literature review US Naval Research Lab Contract No. 4522(00)(X) Narmco Division, The Whittaker Corp
9. Cameron NM (1968) Glass Technol 9:121
10. Charles RJ (1958) J Appl Phys 29:1549. doi:10.1063/1.1722991
11. Charles RJ (1958) J Appl Phys 29:1554. doi:10.1063/1.1722992
12. Metcalfe AG, Shcmitz GK (1972) Glass Technol 13:5
13. Barbero EJ, Damiani TM (2003) J Reinf Plast Compos 22:373. doi:10.1177/0731684403022004269
14. Ray BC (2006) J Colloid Interface Sci 298:111. doi:10.1016/j.jcis.2005.12.023
15. Rao V, Herra-Franco PJ, Ozzelo AD, Drzal LT (1991) J Adhes 34:65. doi:10.1080/00218469108026506
16. Bradley WL, Chiou P, Grant TS (1993) Composite materials for offshore operations. Proceedings of the first international workshop, Texas
17. Drzal LT, Rich MJ, Koenig MF (1985) J Adhes 18:49. doi:10.1080/00218468508074936
18. Schultheisz CR, McDonough WG, Kondagunta S, Shutte CL, Macturk KS, McAuliffe M et al (1996) 13th symposium on composite materials: testing and design
19. Wagner HD, Lustiger A (1994) Compos 25:613. doi:10.1016/0010-4361(94)90192-9
20. Schutte CL, McDonough W, Shioya M, McAuliffe M, Greenwood M (1994) Compos 25:617. doi:10.1016/0010-4361(94)90193-7
21. Pomies F, Carlsson LA (1994) J Compos Mater 28:22
22. Grant TS, Bradley WL (1995) J Comps Mater 29:852
23. Davies P, Pomies F, Carlsson LA (1996) J Comps Mater 30:1004
24. Wood CA, Bradley WL (1997) Compos Sci Technol 57:1033. doi:10.1016/S0266-3538(96)00170-4
25. Fraga AN, Alvarez VA, Vasquez A (2003) J Comp Mater 37:1553. doi:10.1177/0021998303029421
26. Pavlidou S, Krassa K, Papaspyrides CD (2005) J Appl Polym Sci 98:843. doi:10.1002/app.22179
27. Feih S, Wonsyld K, Minzari D, Westmann P, Liholt H (2004) Testing procedure for the single fiber fragmentation test. Riso National Laboratory, Riso-R-483(EN) Roskilde, Denmark
28. Ramirez FA (2008) MS Thesis, Department of Mechanical Engineering, Florida Atlantic University, FL

29. ASTM D3039M-07 (2007) West Conshohocken, PA
30. ASTM D790-07 (2007) West Conshohocken, PA
31. ASTM D638-03 Standard (2003) West Conshohocken, PA
32. ASTM D4065-06 (2006) West Conshohocken, PA
33. ASTM D3379-75 (1975) West Conshohocken, PA
34. ASTM D3171-06 (2006) West Conshohocken, PA
35. Adams DF, Carlsson LA, Pipes RB (2002) Experimental characterization of advanced composite materials, 3rd edn. CRC Press, Boca Raton
36. Kelly A, Tyson WR (1965) J Mech Phys Solids 13:329. doi: 10.1016/0022-5096(65)90035-9
37. Drzal LT, Rich MJ, Camping JD, Park WJ (1980) Proceeding of 35th annual reinforced plastics/composites conference Sect. 20C. The Society of the Plastic Industry, New York, p 1
38. Weibull WJ (1951) J Appl Mech 18:293
39. Timoshenko S (1934) Theory of elasticity, McGraw-Hill
40. Kim BW, Nairn JA (2002) J Compos Mater 36:1825. doi: 10.1177/0021998302036015243
41. Shen CH, Springer GS (1981) In: GS Springer (ed) Environmental effects on composite materials. Technomic, CA
42. Adams DF, King TR, Blackketter DM (1990) Compos Sci Technol 39:341. doi:10.1016/0266-3538(90)90080-O